Study of Voltage Spikes and Temperature Rise in Power Module Based Integrated Converter for 48 V 20 kW Electrically Excited Synchronous Machines

Junfei Tang[*], Yujing Liu[*], Yashovardhan Rastogi[†], Nimananda Sharma[*] and Tanmay Shukla[‡]
Email: {junfei.tang, yujing.liu}@chalmers.se, yashovardhan.rastogi@volvocars.com,
sharman@chalmers.se, tanmay.shukla@segulagrp.com
[*]Division of Electric Power Engineering, Chalmers University of Technology, Gothenburg, Sweden
[†]Volvo Cars Corporation, Gothenburg, Sweden
[‡]Segula Technologies AB, Gothenburg, Sweden

***Abstract*— Electrically Excited Synchronous Motor (EESM) has become an option for electric vehicles, and in order to drive an EESM, an integrated converter is preferred for its compact design so that the machine and the converter can be combined together as a package to deliver power. Therefore, an integrated converter for driving a 48 V 20 kW EESM in mild hybrid applications is designed and tested. Attention is paid to voltage spikes and temperature rises, which are the challenges for a compact design with low voltage but high current ratings. Results show that the idea of integrated converter for EESM is practical and promising. Several suggestions for integrated converter design are given as well.**

Keywords—Electric Machines; Power Electronics; Electrically Excited Synchronous Machines; Integrated Converters

I. INTRODUCTION

Electrically Excited Synchronous Motor (EESM) has become an alternative of Permanent Magnet Synchronous Motor (PMSM) in vehicle applications for its zero permanent magnet consumption, flexibility of power factor control, high efficiency in field weakening operation region and capability of high torque generation during start-up [1] [2]. Besides, EESM offers the possibility of sensorless control by high frequency signal injection on the rotor side [3] [4] [5] [6]. These advantages are due to the fact that EESM provides the control of the field current on the rotor side. The field current can be transferred through a rotating transformer to the rotor side so that brushes and slip rings can be avoided, which makes EESM even more attractive [7] [8].

As for driving electric machines in vehicle applications, an integrated converter is preferred for its high power density, saving of space and components, cost effective and convenience of replacement [9]. In order to drive an EESM, both a three-phase converter to supply the stator winding and an H-bridge converter to supply the field winding are needed. An H-bridge converter integration with the rotor excitation in 48 V mild hybrid vehicles are designed and tested in [10].

However, an integrated design of a three-phase inverter on the stator side together with an H-bridge inverter on the rotor side has not drawn much attention yet. Such integration offers an advantage of sharing the already-existing water cooling system with the motor. Nevertheless, challenges exist as well. For instance, voltage spikes across the switches and temperature rise of the DC-link capacitors are critical. This study therefore investigates a compact design of 48 V 20 kW converter for EESM and focuses on the critical issues of voltage spikes and temperature rise.

II. CONVERTER DESIGN

The power ratings of the converter for driving a 48 V 20 kW EESM are listed in Table I. The stator current RMS values and rotor field current at corresponding power levels are listed respectively. As can be seen, the DC-link voltage is only 48 V whereas the stator current RMS at the peak operation point at 4500 rpm is 477 A, which indicates that the 48 V EESM drive is a low voltage and high current application.

Table I: Converter power ratings for driving the EESM, and the corresponding stator current and rotor current.

Power [kW]		Speed [rev/min]			
		4500		9000	
		$I_{s.rms}$ [A]	I_f [A]	$I_{s.rms}$ [A]	I_f [A]
for Continuous	5	166	7.2	117	5.1
for 30 s	10	281	9.7	197	6.7
for 10 s	15	385	12.1	283	8.8
for 1 s	20	477	15.3	371	11.8

The design of the integrated converter at low voltage but high current ratings faces two challenges: voltage spikes caused by stray inductances and temperature rise caused by losses from the MOSFETs along with the ESR of the DC-link capacitors. The MOSFETs are water cooled since a water cooling system already exists in vehicle applications to cool the motor down. Directly mounting MOSFETs on a water-cooled heat sink is performed in [11] which gives oscillations by high stray inductance. Hence study is pursued by mounting power modules on a water-cooled heat sink in this article. A capacitor PCB is

attached to the power modules from the above, and further above are the driver PCB, H-bridge PCB and DSP board. Components are shown in Figure 1 and the overall view is shown in Figure 2.

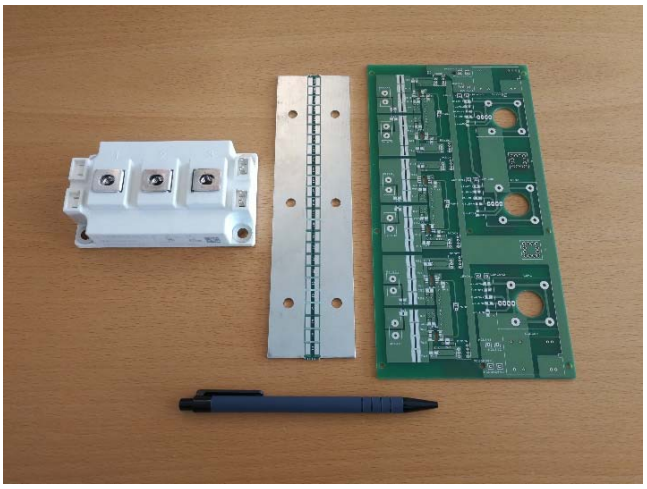

Figure 1: MOSFET power module MD1026HFM150C2S from STARPOWER, capacitor PCB and driver & measurement PCB.

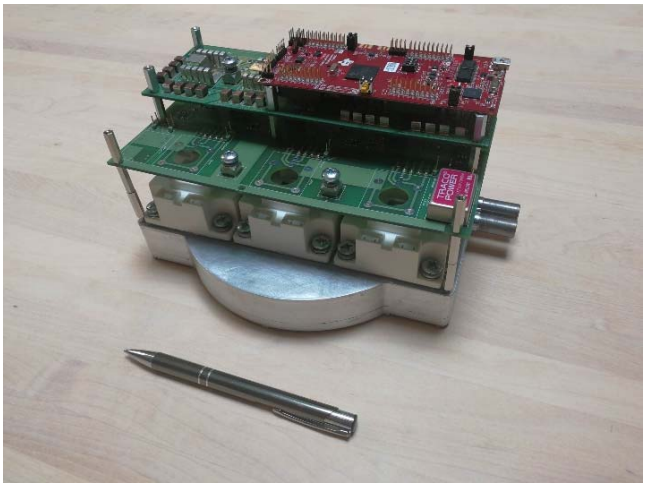

Figure 2: DSP experimental board, H-bridge PCB, driver PCB and MOSFET modules mounted.

III. CONVERTER TEST

A. *Three-Phase Converter with Resistive Load*

The schematic of the three-phase inverter test bench is shown in Figure 3. The DC power from the voltage source is converted to AC power through the inverter, and then the AC power is delivered to a three-phase load through a Δ-Y connected transformer to step up the voltage by a ratio of approximately 10. The photo of the test bench is shown in Figure 4.

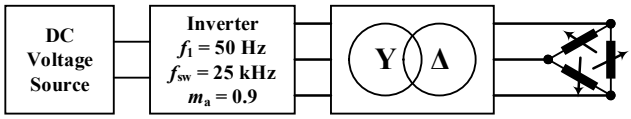

Figure 3: Schematic of three-phase inverter test bench.

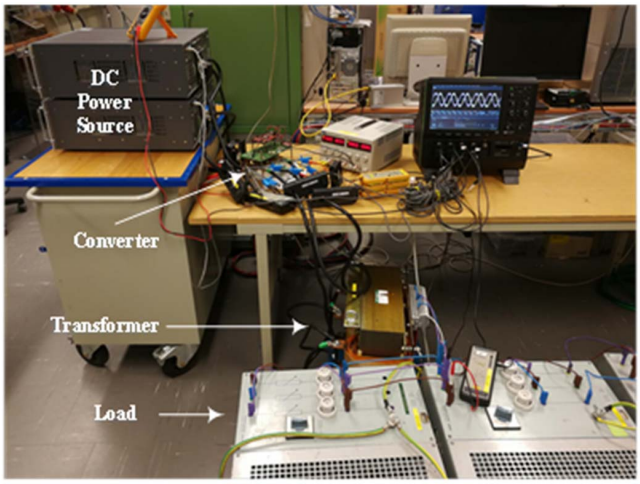

Figure 4: Photo of the test bench.

In order to test the three-phase inverter, firstly a test with 5 kW continuous output is performed, which is denoted as Test 1 in this article. Output voltages and currents are shown in Figure 5 and Figure 6 respectively. As can be seen, the currents are quite sinusoidal and the voltage spikes of around 50 V give maximum phase peak voltages of 100 V which are lower than the breakdown voltage of 150 V. Figure 7 shows the DC-link voltage and current. The current ripple is around 25 A and the voltage spikes are less than 10 V. These are due to the fact that no input filter is applied for the converter. Figure 8 shows the temperature of the converter in steady state. And as can be noticed, the highest temperature appears on the capacitors and it is far below the 125 °C temperature limit of the capacitors. Hence it can be concluded up to here that the converter is suitable for continuous operation.

As has been mentioned, the two main problems are voltage spikes and temperature rise. Therefore, two additional tests at approximately 10 kW for 30 s are conducted: higher voltage and lower current are applied in Test 2 to check over voltage capability whereas lower voltage and higher current are applied in Test 3 to check over temperature capability. The results of all the three tests are shown in Table II. As can be noticed, by comparing Test 2 and 3, to deliver almost the same power output, efficiency reduces at higher current instead of higher voltage.

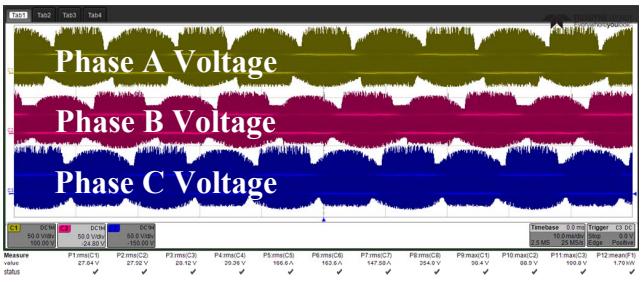

Figure 5: Output voltages: yellow, red and blue are Phase A, B and C to N respectively. Scale is 50 V / div.

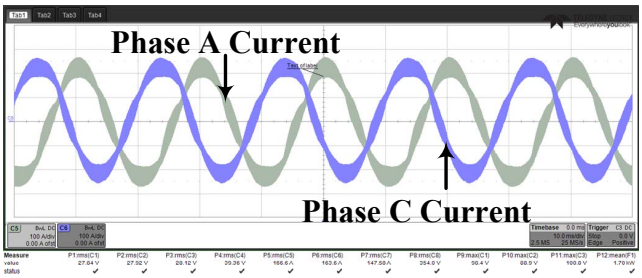

Figure 6: Output currents: grey is Phase A and purple is Phase C. Scale is 100 A / div.

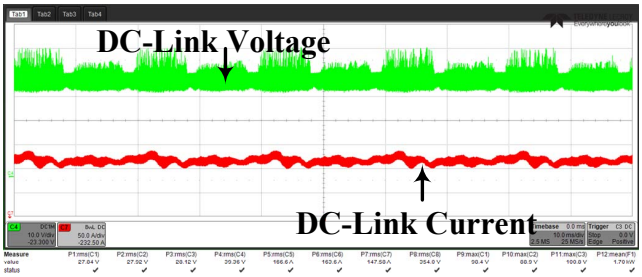

Figure 7: DC-link voltage and current. Scales are 10 V / div and 50 A / div.

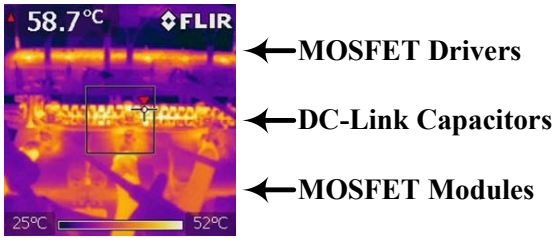

Figure 8: Temperature in steady state with ambient temperature of around 22 °C

The voltage variations are compared in Figure 9. As can be noticed, in both cases, the phase voltage spikes are much higher than DC-link voltage spikes. In addition, a reduction of current does not reduce the DC-link voltage spikes very much but reduces the phase voltage spikes. These can be explained in

Figure 10, where $L_{dc.\sigma.1} \sim L_{dc.\sigma.12}$ are the stray inductance along the bus bar, $L_{A.\sigma.1} \sim L_{A.\sigma.4}$, $L_{B.\sigma.1} \sim L_{B.\sigma.4}$ and $L_{C.\sigma.1} \sim L_{C.\sigma.4}$ are the stray inductance inside the power module. The capacitance along the DC-link $C_{dc.A}$, $C_{dc.B}$ and $C_{dc.C}$ stabilize the voltage at the terminals of the power module, i.e. the DC-link voltage, but cannot eliminate the voltage spikes caused by stray inductance inside the power module. Therefore, a lower output current reduces di/dt and further reduces the voltage spikes. One suggestion is to select MOSFETs with high breakdown voltage, and another is to increase the gate resistance to decrease di/dt.

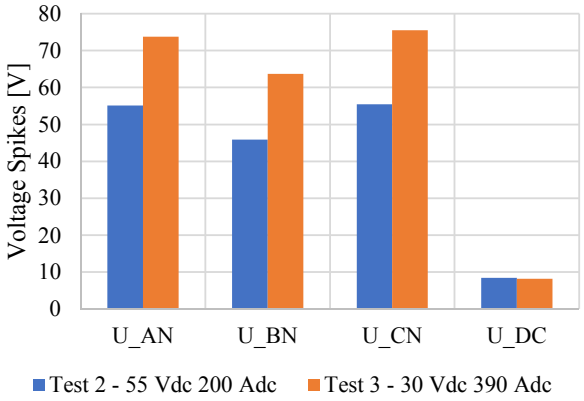

Figure 9: Voltage variation of Test 2 and 3.

Figure 11 shows the temperature variation along the DC-link capacitors in Test 2, where capacitors close to Phase B give the highest temperature. The explanation can be illustrated in Figure 12. The commutation currents between all the three phases need to pass through the capacitors in the middle, and the concentration of commutation currents causes the uneven temperature distribution. More capacitors are therefore suggested to be placed in the middle of the bus bar.

Table II: Test results: Test 1 at around 5 kW for continuous operation, Test 2 & 3 at around 10 kW for 30 s.

	U_{DC} [V]	I_{DC} [A]	P_{DC} [kW]	$U_{line.rms.avg}$ [Vrms]	$I_{rms.avg}$ [Arms]	P_{AC} [kW]	Q_{AC} [kVar]	S_{AC} [kVA]	η [%]
Test 1	39.3	147.5	5.8	27.0	162.0	5.6	5.1	7.6	96.7
Test 2	55	200	11.0	37.7	209.9	10.3	9.0	13.7	93.9
Test 3	30	390	11.7	19.5	418.9	9.5	10.4	14.1	81.6

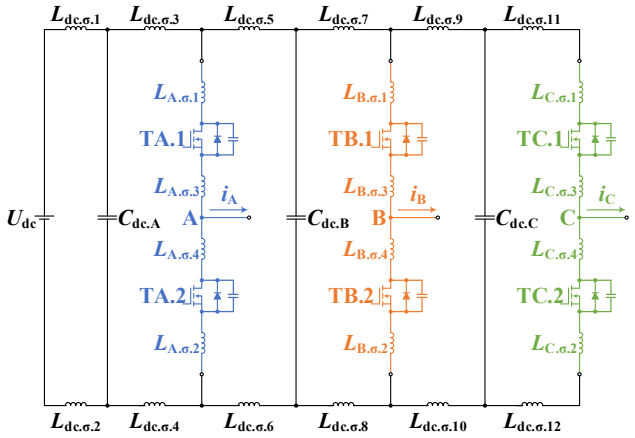

Figure 10: Internal stray inductance that causes voltage pikes.

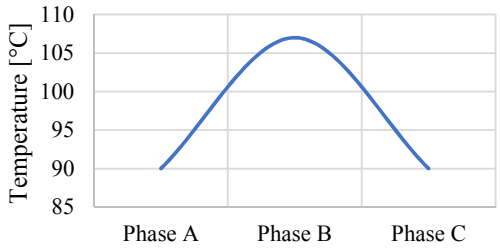

Figure 11: Temperature distribution along the DC-link capacitor bank.

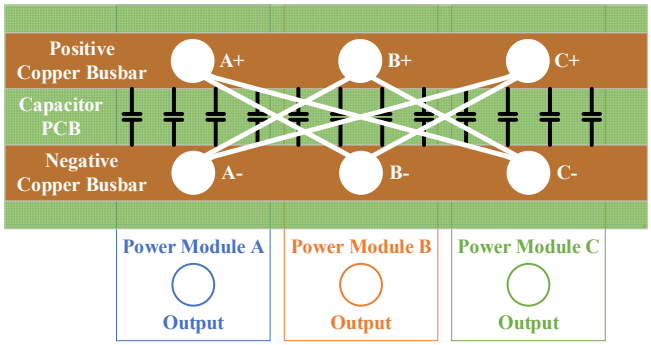

Figure 12: Commutation current concentrated on the capacitors in the middle of the DC-link.

B. H-Bridge Converter with Rotating Transformer

The H-Bridge converter is used to excite the rotor winding and the circuit of the rotor excitation is shown in Figure 13. The H-Bridge converter is composed of three parts, an H-Bridge inverter, a rotating transformer and a rectifier. The H-bridge inverter generates AC power and the AC power is transferred from the primary side to the secondary side of the transformer through the air gap. Then, the AC power is converted to DC power through a rectifier and gives field current flowing in the rotor winding. In the figure, TA+, TA-, TB+ and TB- are the switches of the H-Bridge converter, $L_{1\sigma}$, $L_{2\sigma}$ and L_M are the primary and secondary side leakage inductances and the magnetizing inductance of the rotating transformer respectively, DA+, DA-, DB+ and DB- are the diodes of the Rectifier.

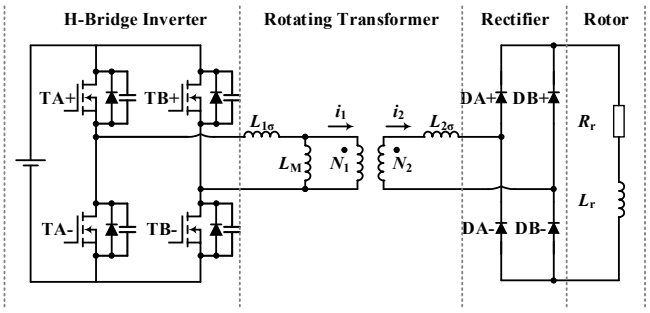

Figure 13: Rotor excitation circuit.

For a better understanding of the circuit, the schematic of the rotor excitation circuit is shown in Figure 14. The primary side of the transformer is stationary whereas the secondary side is rotary. The rectifier is attached to the back of the secondary side of the transformer.

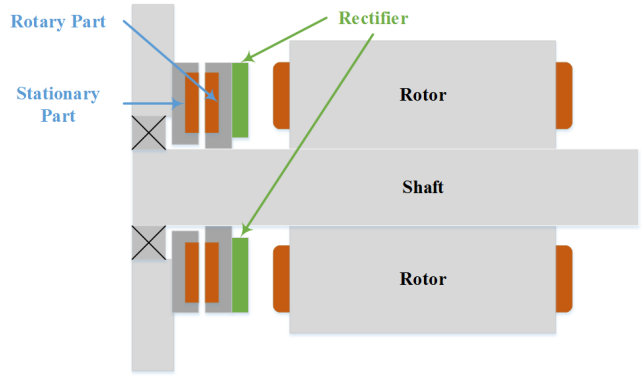

Figure 14: Schematic of the rotor excitation circuit.

Figure 15 shows the design of the rotating part of the transformer and the rectifier. An aluminum case is designed as shown in (a) and the diodes are connected through a PCB which covers the aluminum case after assembly as shown in (b). As can be noticed, slots are cut so that

- The area for heat dissipation is maximized without making the geometry too complicated.
- Ventilation can be generated through the slots at rotation.

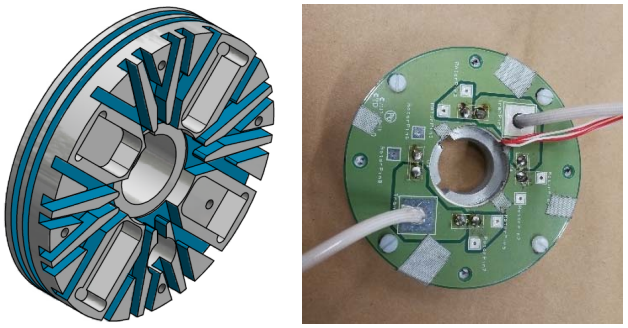

(a) (b)

Figure 15: Field winding rectifier.

Figure 16 shows the photo of the test bench of the excitation circuit. Voltages and currents at DC-link, primary and secondary sides of the transformer and the field windings are measured. In addition, the temperatures at the transformer windings, stator windings, rotor windings are recorded through the PT100 temperature sensors installed inside the windings.

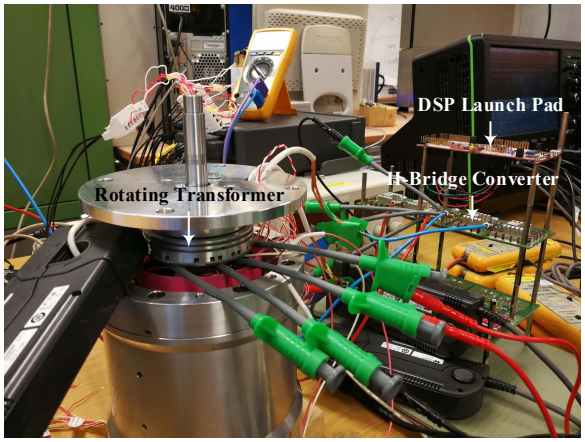

Figure 16: Test of the excitation circuit.

1) Application of ZVS and Loss of Duty Cycle

The phase-shift modulation technique is applied to generate the switching signals to achieve zero voltage switching (ZVS). Two criteria determine the condition of ZVS:

- Inductive energy storage in the transformer is larger than the capacitive energy storage in the parasitic capacitance of the switches.
- Blanking time is long enough for the energy transferring from the inductance to the capacitance.

In this design, the blanking time is selected as 100 ns and ZVS is achieved for the duty cycle from 0.1 to 1.

The application of ZVS is necessary in EESM excitation. A comparison has been done between non-ZVS and ZVS by connecting the converter to two versions of transformers as shown in Figure 17. (a) is the case with a smaller inductance and ZVS is not achieved in one leg of the converter, whereas (b) is the case with a larger inductance and ZVS is achieved in both legs. Both cases are at natural ventilation. As can be noticed, ZVS can reduce the temperature rise significantly. In addition, it has also been observed that under ZVS, the temperature rise is almost constant regardless of the duty cycle, whereas in the case of non-ZVS, the temperature is duty cycle dependent. The explanation of the importance of ZVS is that at the switching frequency of 100 kHz, the switching loss is significant and as for low voltage MOSFETs, the $R_{ds(on)}$ is quite small (1.7 mΩ in this design) which means the conduction loss is negligible. Therefore, in the H-Bridge converter for EESM rotor excitation, the application of ZVS is essential since it can reduce the switching loss significantly. A wider range of ZVS is preferred.

Figure 18 shows the voltage and current waveforms of both sides of the transformer. Three phenomena can be observed:

- The spikes of the H-bridge converter output are negligible. It is safe to select a MOSFET with a break down voltage of 100 V in the 48 V application.
- Ringing can be observed at the rectifier input.
- The duty cycle of the primary side is 100%, i.e. 50% positive output and 50% negative output in one switching cycle, whereas the secondary side is only 60%, i.e. 30% positive output and 30% negative output in one switching cycle. This phenomenon is referred to as duty cycle loss of phase-shift controlled H-Bridge converters.

The explanations of the ringing and the loss of duty cycle are given as follows.

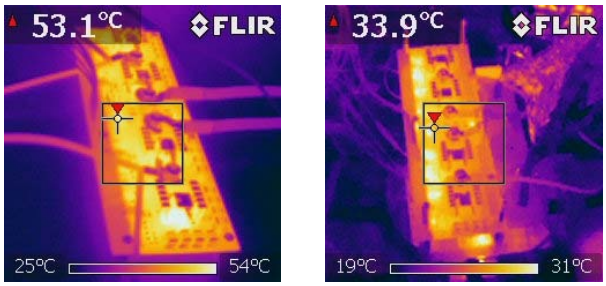

(a) (b)

Figure 17: Thermal photo of the H-Bridge converter: (a) non-ZVS; (b) ZVS. The ambient temperature is 22 °C

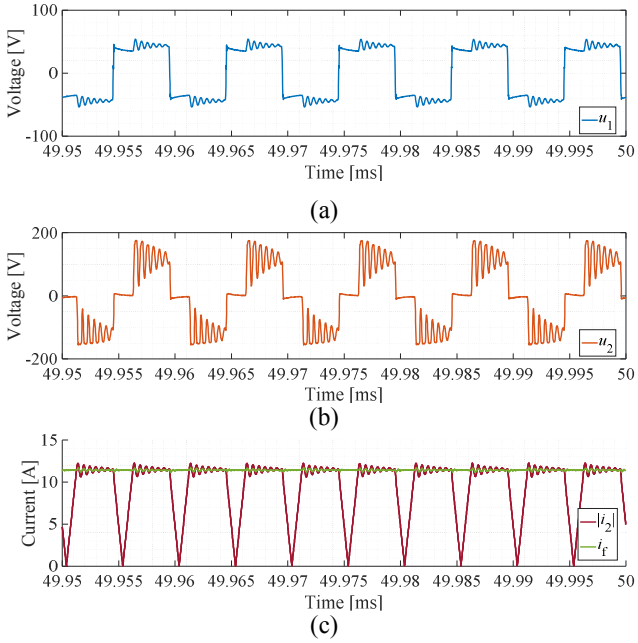

Figure 18: Spikes, ringing and duty cycle loose of the H-Bridge excitation circuit: (a) transformer primary side voltage, i.e. H-Bridge converter output voltage; (b) transformer secondary side voltage, i.e. rectifier input voltage; (c) absolute value of the transformer secondary side current and field current.

The turn-on transient of the switch is illustrated in Figure 19. In (a), before the turning on of TA-, the anti-parallel diode of TA- conducts current, and since the transformer current is going to be reversed, the current going through the transformer is

decreasing. However, since the field current is a DC quantity, the sum of i_{DA+} and i_{DB+} must be constant. Then the decrease of the transformer current, i.e. i_{DA+}, must be compensated by introducing i_{DB+}, which means that both DA+ and DB+ must conduct current. This further indicates that a short circuit of the secondary side of the transformer is introduced. Therefore, the output voltage of the transformer is clamped to zero by the short-circuit of the rectifier.

Then, in (b), TA- is turned on, but the short-circuit still continues until the transformer current reverses in (c) and reaches the field current level in (d), and after that, the DB+ and DA- path can feed enough current to the field winding which means DA+ and DB- shut down and the short circuit disappears. This explanation can be verified in the test result shown in Figure 18 (b) and (c). As can be seen, the duty cycle on the secondary side remains zero until the absolute value of the secondary side current reaches the field current.

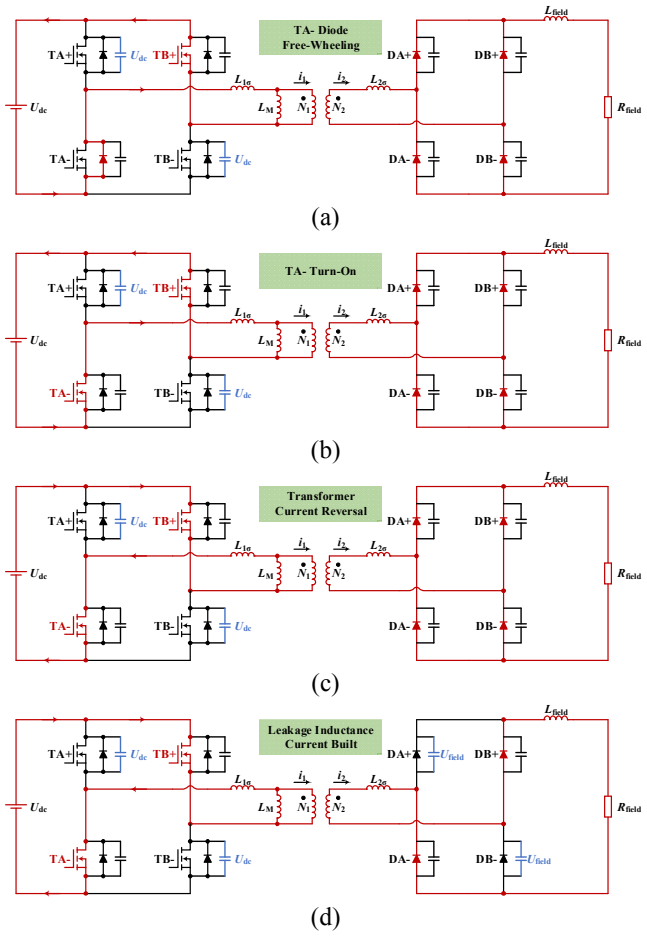

Figure 19: Explanation for the duty-cycle loss and ringing.

The duty cycle loss reduces the power transfer from the primary side to the secondary side and is therefore definitely not preferable. As can be noticed, the loss of duty cycle on the secondary side is during Mode (b) and (c) in Figure 19, and the duration of the duty cycle loss depends on how fast the transformer current can be reversed. And during (b) and (c),

$$u_{dc} = \left[L_{1\sigma} + L_M // \left(\frac{{N_1}^2}{{N_2}^2} L_{2\sigma}\right)\right] \frac{di_1}{dt} \approx L_{1\sigma} \frac{di_1}{dt}. \qquad (1)$$

Hence a higher dc-link voltage and a lower leakage-inductance can give a quicker current reverse and therefore a shorter loss of duty cycle. However, a lower leakage-inductance means a lower energy storage in the inductance and due to the criteria of ZVS, a lower leakage-inductance will reduce the range of ZVS, i.e ZVS cannot be achieved at a higher current level than in a higher self-inductance case. Hence one important issue that should be considered is the trade-off between the loss of duty cycle on the secondary side and the ZVS range.

As for the ringing, it should be due to the oscillation between the inductance (field winding inductance + transformer leakage inductance) and the parasitic capacitance of the diodes in the rectifier. From Figure 18 (c) to (d), the parasitic capacitance of the diodes are charged from zero to U_{field}, and since the capacitance is charged through inductive current, LC resonance will happen. In order to deal with the ringing, one way to add capacitance at the output of the rectifier to smooth the voltage and reduce the ringing. The other way is to keep the system simple, and use at least twice of the field winding voltage level as the diode break down voltage on the secondary side of the transformer.

2) Step Response Test of the Excitation Circuit

A series of step response tests of the field current have been done at standing still. The reasons of performing step response tests are

- The 48 V EESM in mild hybrid vehicle is used for start-up acceleration and a step of the field current is an imitation of the acceleration situation.
- The rise time and the field current / dc-link input current ratio of the excitation circuit at different temperatures can be observed and compared.

Figure 20 shows the temperature record during the step response tests. The steps are started at a temperature from 22 °C up to 120 °C. The blue and orange curves represent the temperatures of the transformer primary and secondary windings respectively, and the red curve represents the average current of the field windings under each pole. As can be noticed, during the test, the field winding temperature shoots up more swiftly compared with the transformer winding. And, the temperature of the H-bridge inverter is far lower as shown in Figure 17 (b). It is therefore concluded that, when ZVS is applied, the temperature rise is much more critical in the field winding instead of the H-Bridge inverter and the transformer.

Figure 21 shows the step response of the field current at 120 °C. The duty cycle of the H-Bridge jumps from 0 to 1 at 9 ms, and the rise time of the field current along with the dc-link input current is 18.3 ms. This time length is considered as short enough to start up the vehicle.

Figure 22 (a) shows the ratio between the dc-link current input of the excitation circuit and the field current, i.e. the ratio

between the output DC current and the input DC current. The ratio is changed by the temperature rise from 1.65 to 1.82 with the mean value of 1.73. Figure 22 (b) shows the rise time at each temperature which varies from 18.1 to 18.7 ms. As can be seen, the temperature rise of the excitation circuit has no significant impact on either the ratio or the rise time.

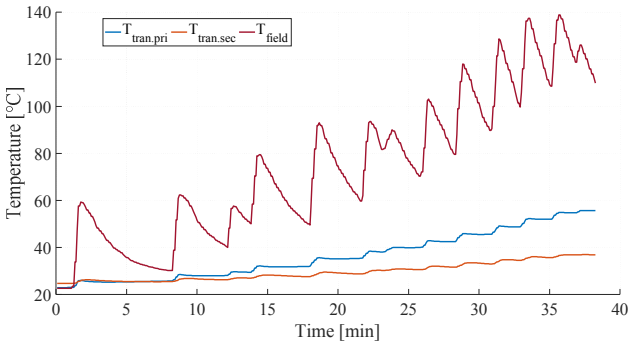

Figure 20: Temperature record of the step test at standing still.

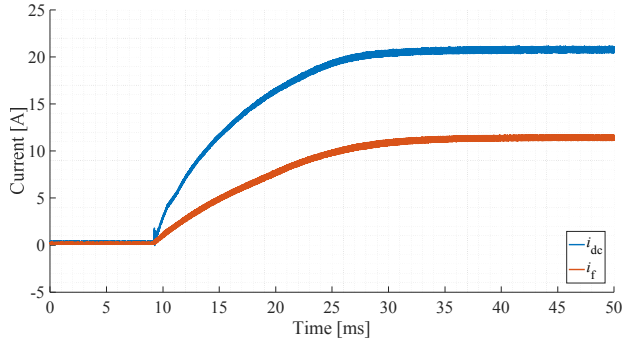

Figure 21: Step response of the excitation circuit.

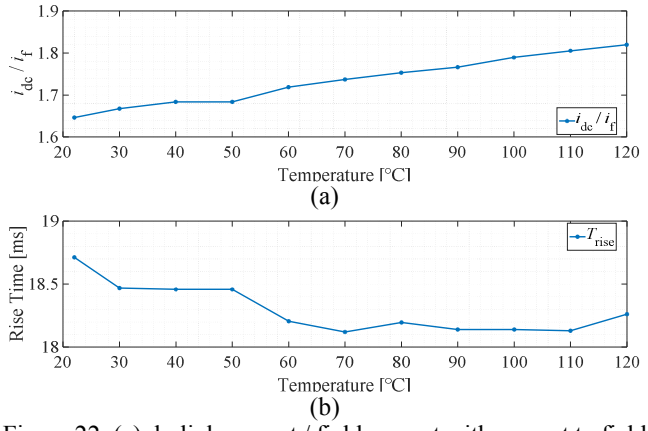

Figure 22: (a) dc-link current / field current with respect to field winding temperature; (b) rise time with respect to field winding temperature.

IV. INTEGRATION DESIGN

A. *Difficulty of Integration in Current Version*

The current version of the converter was intended to be placed at the end cover of the EESM. However, due to the bulky volume of the power module, the parallel layout of the power modules becomes larger than the end cover. Therefore, the target of the current version is redefined to verify the performance of the converter, e.g. voltage spikes, temperature rise and electromagnetic interference.

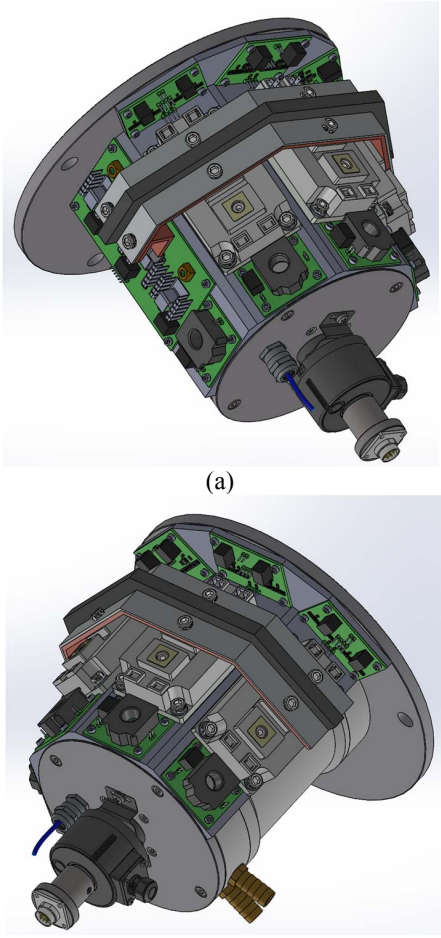

(a)

(b)

Figure 23: Design of the integrated converter: (a) Left Isometric View; (b) Right Isometric View.

B. *CAD Design of New Version*

The design of a new version of integrated converter has started. The left and right isometric views are shown in Figure 23 (a) and (b) respectively. The PCBs are avoided to be placed one above another in order to deal with the EMI challenges. As for the three-phase inverter, the power modules are attached to the radial housing of the motor and therefore share the cooling jacket with the motor. The gate drivers for the power modules are fixed to the end plate of the motor with M3 screws which are perpendicular to the power module. This design is to minimize the distance between the driver and the power module within

limited space. The H-Bridge inverter is placed on a PCB similar to the current design and is beside the power modules. In order to save space, the H-Bridge inverter share the DC-link capacitors with the three-phase inverter.

Since the power modules are not on the same plane, the DC-link capacitors have to be populated on several PCBs instead of one. Two copper bus bars, one positive and one negative, are used to conduct DC-link current and placed under the DC-link capacitor PCBs. The capacitor PCBs are fixed to the copper bus bar with M6 screws. In the CAD drawing, the capacitors are presented as gray tubes because it has not been decided whether to use ceramic capacitors or to use customized film capacitors. The current sensor for each module is placed on the same plane of the module. The output cable from each module will go through the current sensor and into the motor housing directly.

V. Conclusions and Future Work

The strategy to design a low voltage and high current converter by utilizing power modules is generally successful. The EESM has been assembled and the test of the converter together with the EESM as a system is going on.

As for the three-phase inverter, the voltage spikes are mainly caused by the stray inductance inside the power modules. One suggestion is to select MOSFETs of higher breakdown voltage, and another is to increase the gate resistance. As for a parallel placement of power modules, more capacitors are suggested to be placed in the middle of the bus bar to ease the concentration of the commutation current.

As for the field excitation, the voltage spikes at the output of the H-Bridge inverter is negligible, and if ZVS is applied, the temperature rise of the H-Bridge inverter is limited. However, the implementation of ZVS and the loss of duty cycle should be traded off. In addition, the voltage ringing at the input of the rectifier is severe. One solution is to add a capacitor at the output of the rectifier and another solution is to select diodes with a higher breakdown voltage level. A proper design of the transformer heatsink helps limit the temperature rise of the transformer windings. The temperature rise of the excitation circuit does not affect either the response of the field current or the input / output current ratio very much.

References

[1] G. Friedrich, "Experimental comparison between Wound Rotor and permanent magnet synchronous machine for Integrated Starter Generator applications," in *2010 IEEE Energy Conversion Congress and Exposition (ECCE)*, 2010.

[2] D. G. Dorrell, "Are wound-rotor synchronous motors suitable for use in high efficiency torque-dense automotive drives?," in *IECON 2012 - 38th Annual Conference on IEEE Industrial Electronics Society*, Montreal, QC, Canada, 2012.

[3] J. Choi, I. Jeong, K. Nam and S. Jung, "Sensorless control for electrically energized synchronous motor based on signal injection to field winding," in *IECON 2013 - 39th Annual Conference of the IEEE Industrial Electronics Society*, Vienna, Austria, 2013.

[4] S. Choe, E. Jung and S.-K. Sul, "Sensorless Control of Synchronous Machine With an Inverter Integrated Rotor," *IEEE Transactions on Industry Applications,* vol. 50, no. 4, pp. 2584 - 2591, 2013.

[5] Y. Zhou and S. Long, "Sensorless Direct Torque Control for Electrically Excited Synchronous Motor Based on Injecting High-Frequency Ripple Current Into Rotor Winding," *IEEE Transactions on Energy Conversion,* vol. 30, no. 1, pp. 246 - 253, 2014.

[6] S. Feuersänger and M. Pacas, "Rotor position identification in synchronous machines by using the excitation machine as a sensor," in *2016 IEEE Symposium on Sensorless Control for Electrical Drives (SLED)*, Nadi, Fiji, 2016.

[7] C. Stancu, T. Ward, K. Rahman, R. Dawsey and P. Savagian, "Separately excited synchronous motor with rotary transformer for hybrid vehicle application," in *2014 IEEE Energy Conversion Congress and Exposition (ECCE)*, Pittsburgh, PA, USA, 2014.

[8] Y. Liu, D. Pehrman, O. Lykartsis, J. Tang and T. Liu, "High frequency exciter of electrically excited synchronous motors for vehicle applications," in *2016 XXII International Conference on Electrical Machines (ICEM)*, Lausanne, Switzerland, 2016.

[9] M. Schier, F. Rinderknecht and N. S. Kumar, "Highly integrated Electric Drives for Automotive Application," in *Renewables and Technology (SMART), 2015 International Conference on Sustainable Mobility Applications*, Kuwait City, Kuwait, 2015.

[10] S. Saponara, P. Tisserand, P. Chassard and D.-M. Ton, "Design and Measurement of Integrated Converters for Belt-Driven Starter-Generator in 48 V Micro/Mild Hybrid Vehicles," *IEEE Transactions on Industry Applications,* vol. 53, no. 4, pp. 3936 - 3949, 2017.

[11] F. Fürst, "Design of a 48 V three-phase inverter for automotive applications," Chalmers University of Technology, Gothenburg, 2016.